

Supporting information

Porous Bipolar Polymers as Organic Cathodes for Sustainable Sodium/Potassium-ion Batteries

Motahareh Mohammadiroudbari,^a Jinghao Huang,^a Eric Youngsam Kim,^a Zhenzhen Yang,^b Fu Chen,^c and Chao Luo^{*a,d}

^aDepartment of Chemistry and Biochemistry, George Mason University, Fairfax, VA, 22030, USA

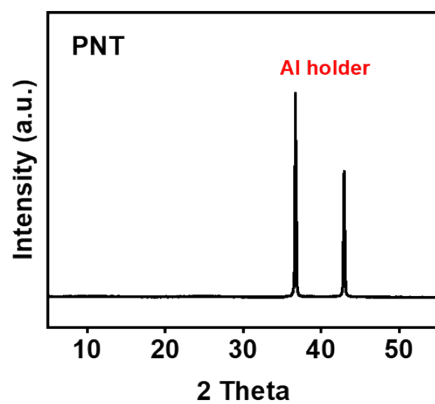
^bMaterials Science Division, Argonne National Laboratory, Lemont, IL, 60439, USA

^cDepartment of Chemistry and Biochemistry, University of Maryland, College Park, MD, 20742, USA

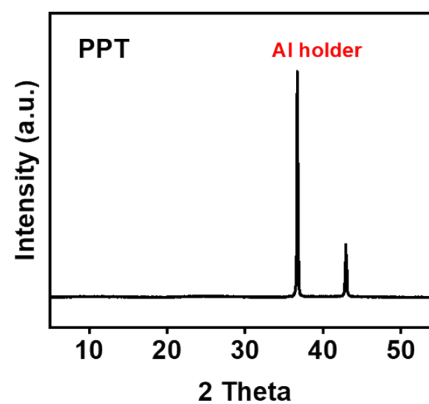
^dQuantum Science & Engineering Center, George Mason University, Fairfax, VA, 22030, USA

*Corresponding author: cluo@gmu.edu

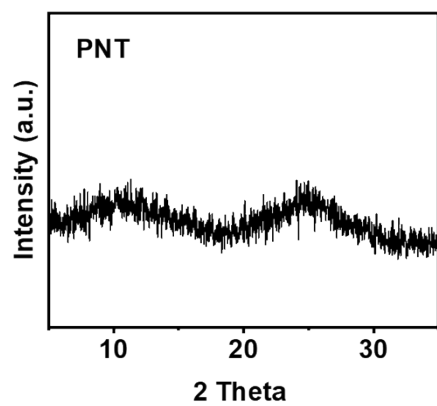
(a)



(b)



(c)



(d)

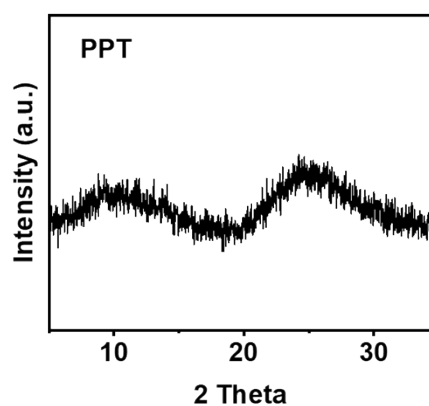
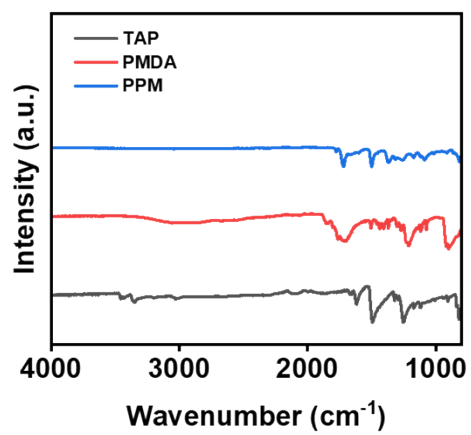


Fig. S1 XRD spectra for PNT and PPT.

(a)



(b)

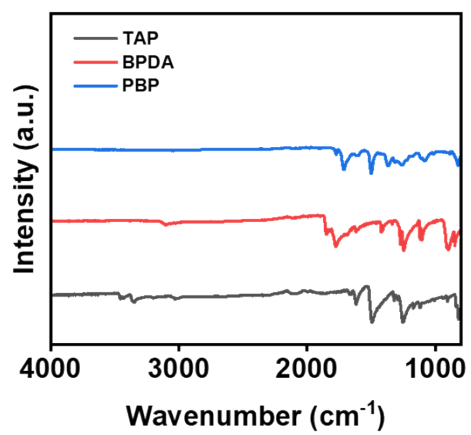


Fig. S2 FTIR spectra for PPM and PBP.

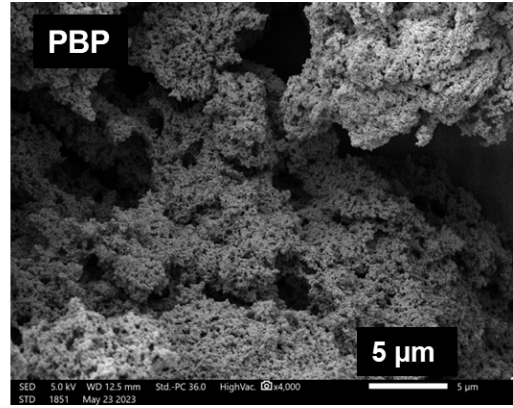
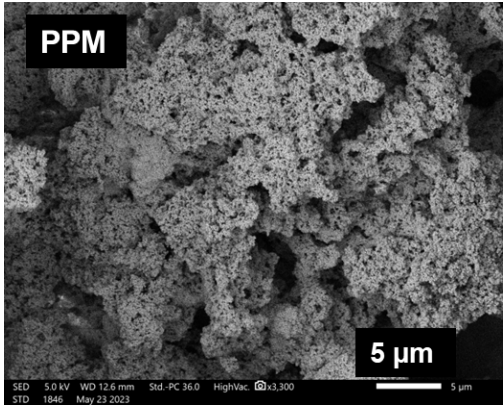


Fig. S3 SEM images for PPM and PBP

Table S1 BET results for the four mesoporous polymers.

Measurement	Polymers	PNT	PPT	PMP	PBP
BET surface area (m²/g)		167.00	1.22	312.58	187.33
Adsorption average pore diameter (nm)		5.26	13.6	6.27	11.71
Desorption average pore diameter (nm)		5.59	10.2	6.21	11.64

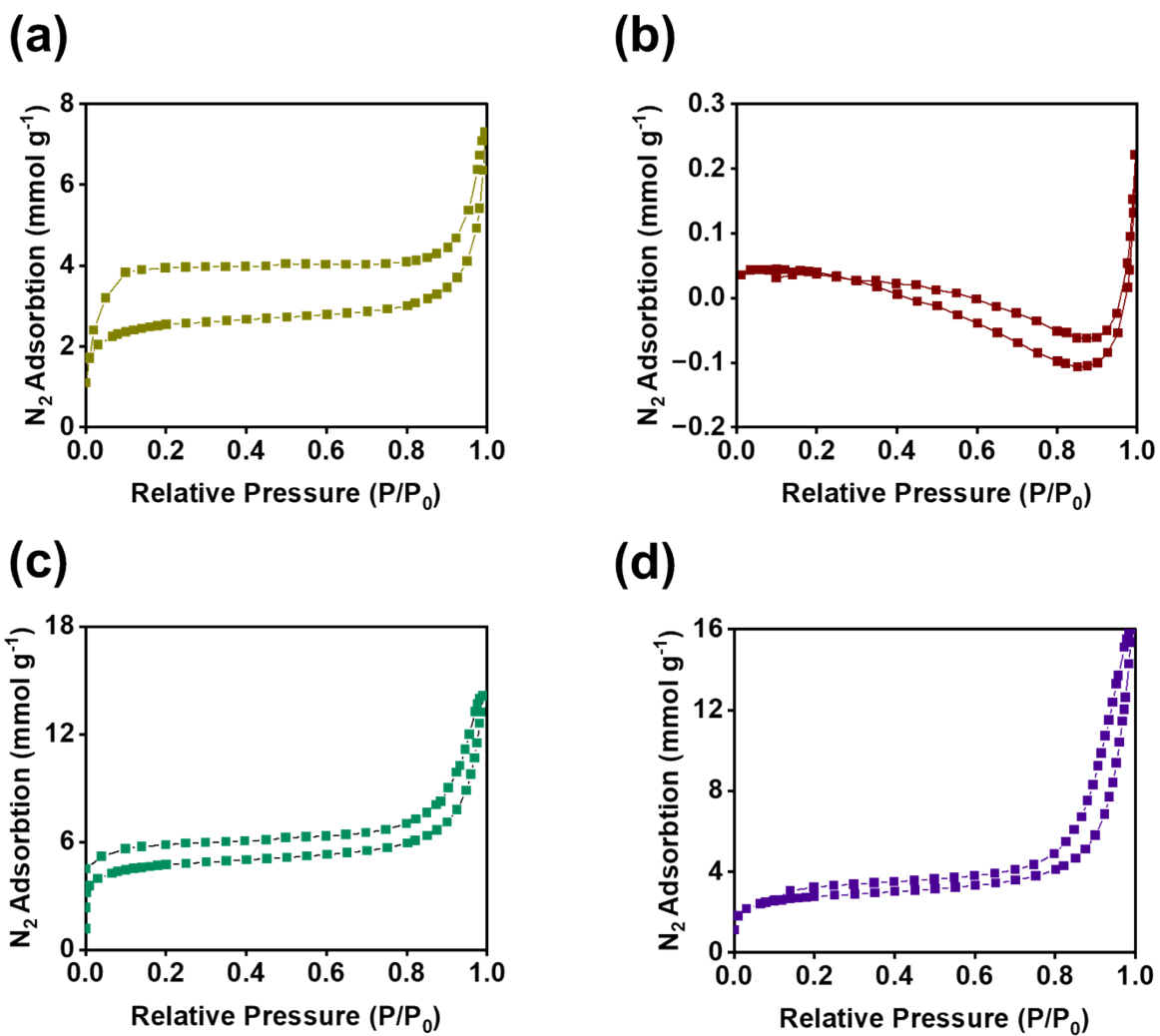


Fig. S4 Adsorbed N_2 as a function of relative pressure for mesoporous polymers: (a) PNT, (b) PPT, (c) PPM, (d) PBP.

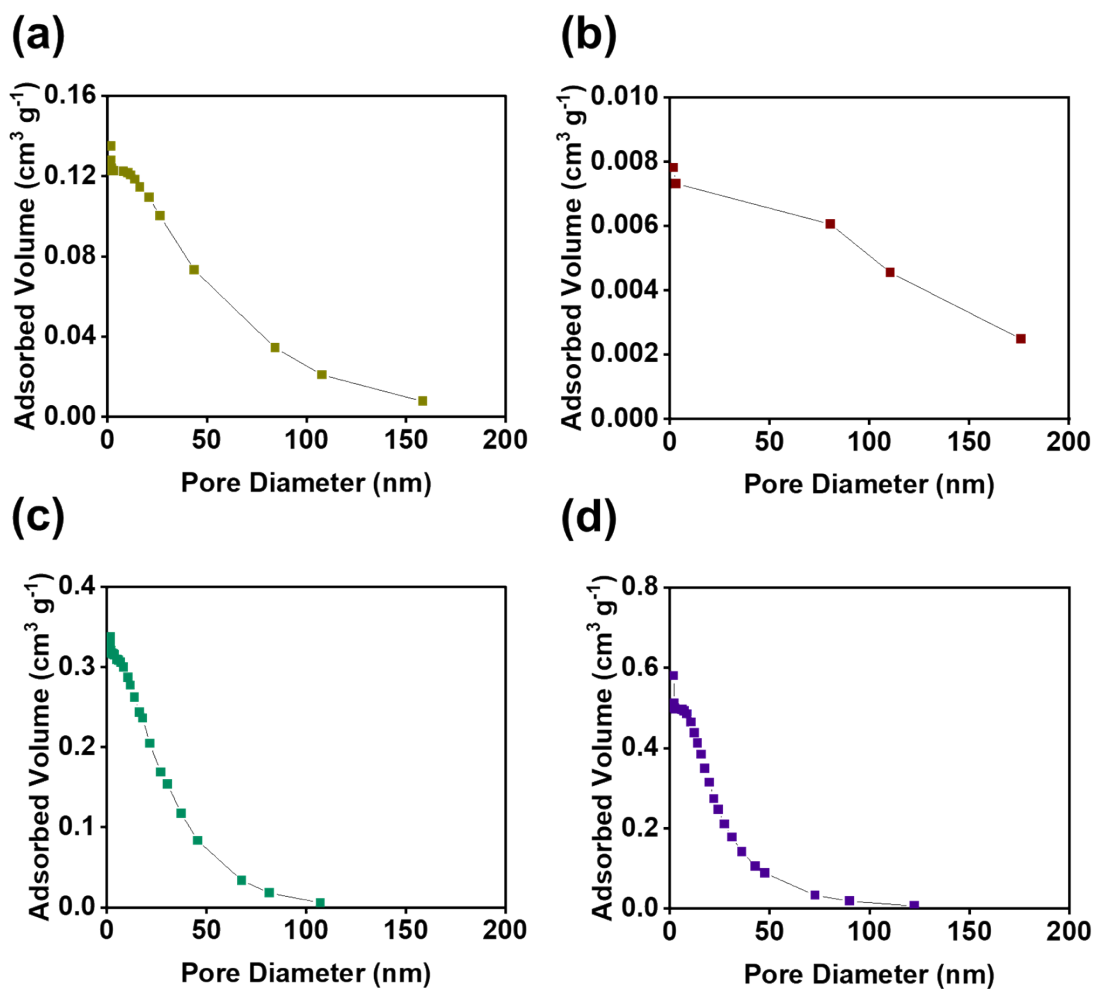


Fig. S5 Pore size distribution for mesoporous polymers: (a) PNT, (b) PPT, (c) PPM, (d) PBP.

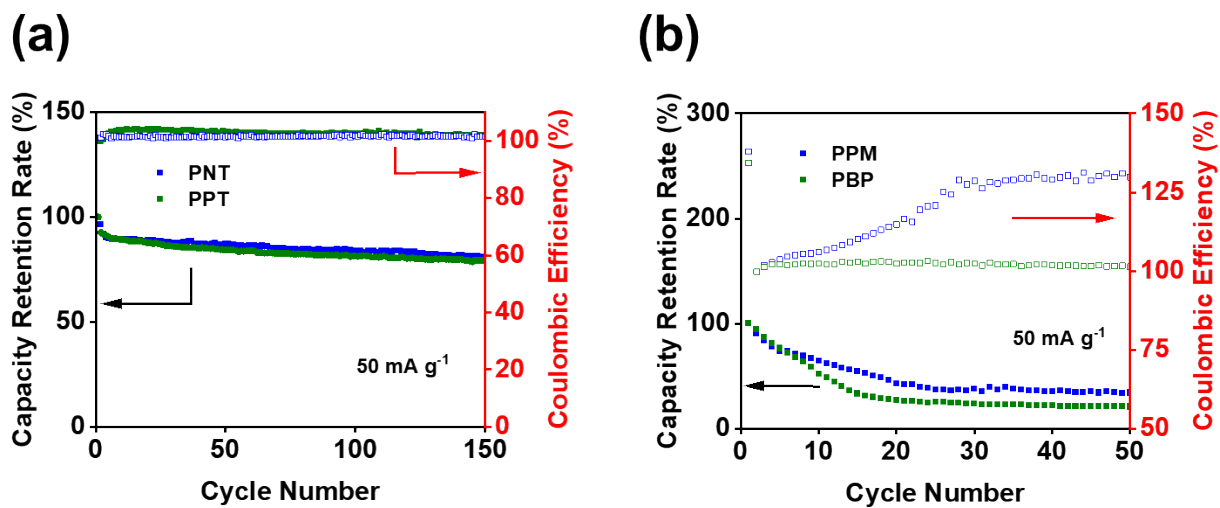


Fig. S6 Capacity retention in NIBs: (a) PNT and PPT, (b) PPM and PBP.

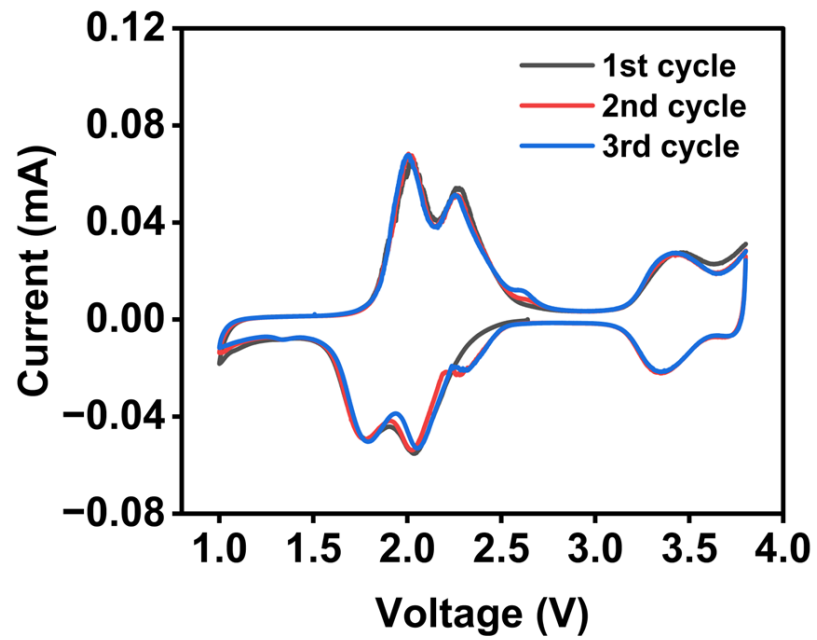


Fig. S7 Cyclic voltammogram for PNT/single-layer graphene at the scan rate of 0.1 mV s^{-1} in NIBs.

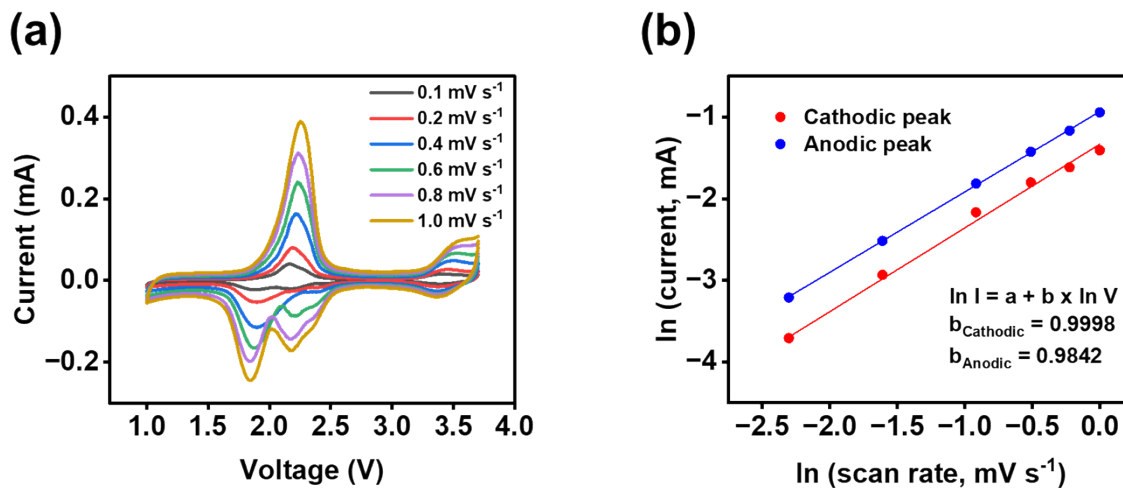
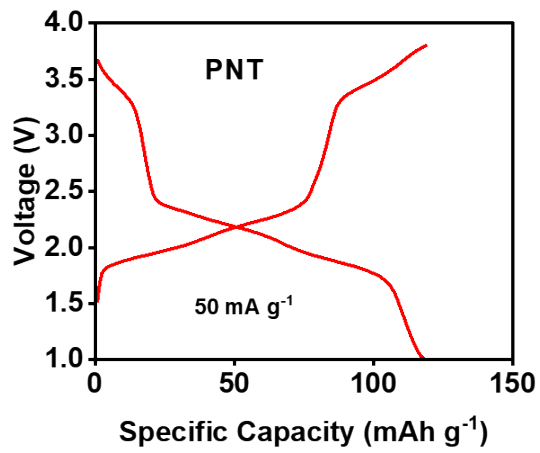


Fig. S8 Reaction kinetics for PPT/single-layer graphene in NIBs: (a) cyclic voltammograms at scan rates of 0.1-1 mV s⁻¹, (b) the natural logarithm of peak current versus scan rate.

(a)



(b)

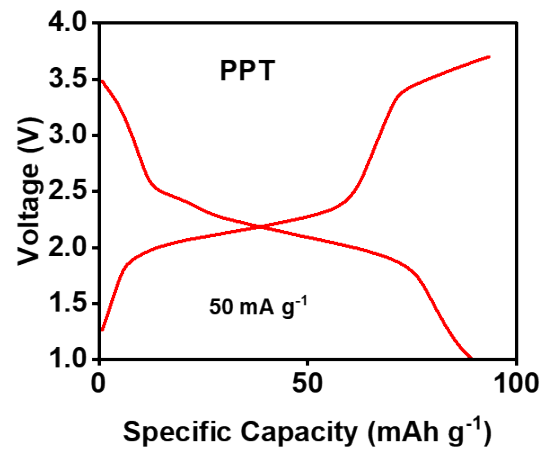


Fig. S9 Galvanostatic charge–discharge curves at the 150th cycle in NIBs: (a) PNT, (b) PPT.

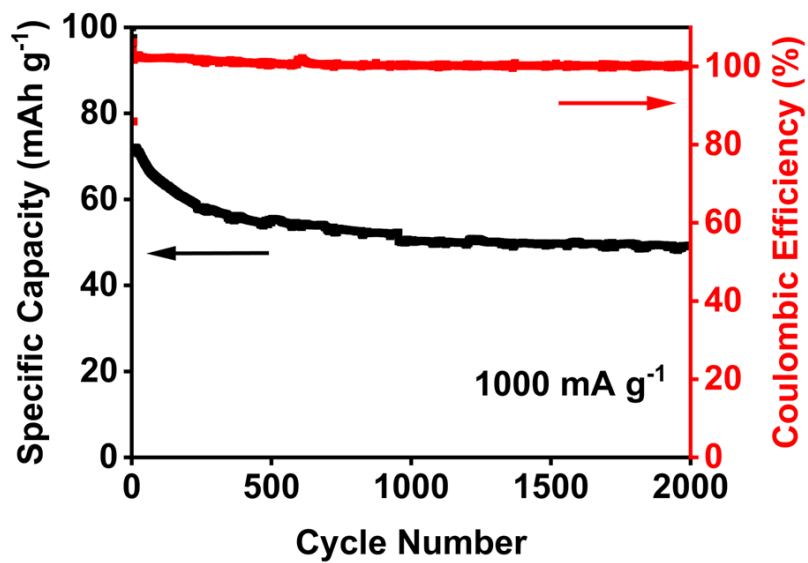


Fig. S10 De-sodiation capacity and Coulombic efficiency for PPT/single-layer graphene at the scan rate of 1,000 mA g⁻¹ in NIBs.

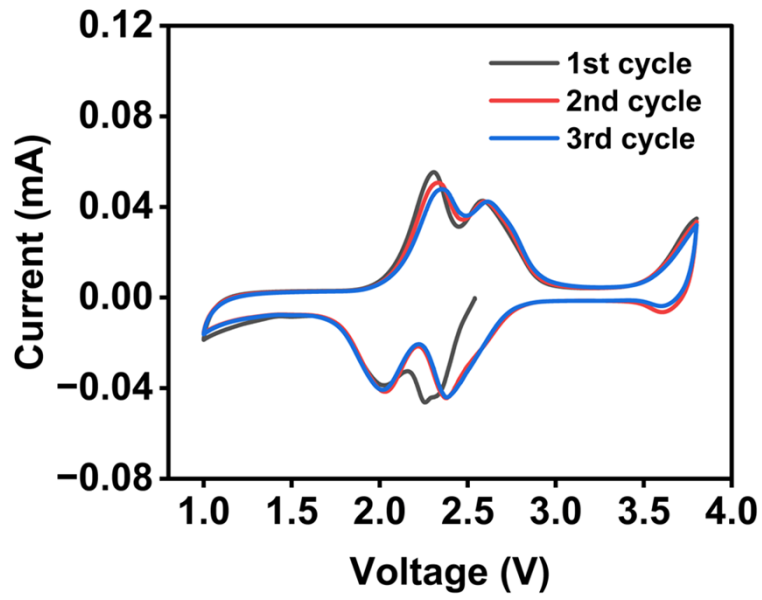


Fig. S11 Cyclic voltammogram for PNT/single-layer graphene at the scan rate of 0.1 mV s^{-1} in KIBs.

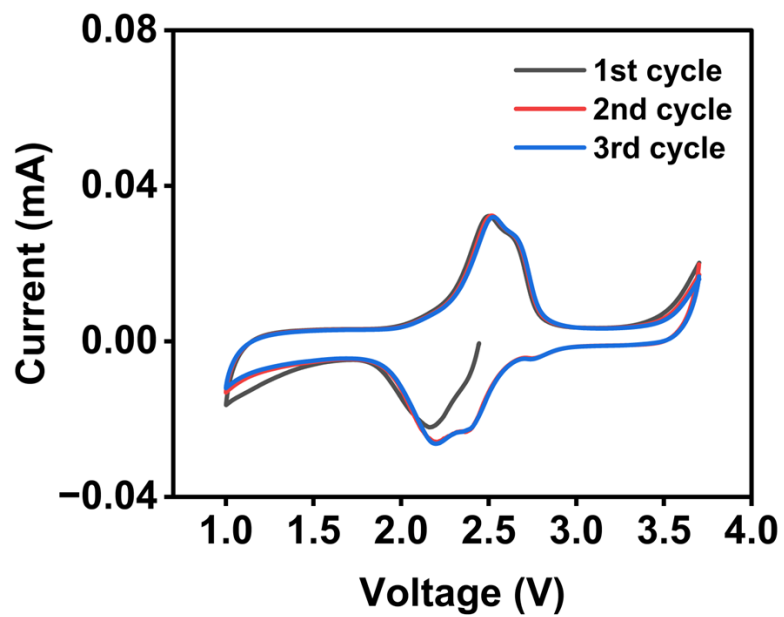


Fig. S12 Cyclic voltammogram for PPT/single-layer graphene at scan rates of 0.1 mV s^{-1} in KIBs.

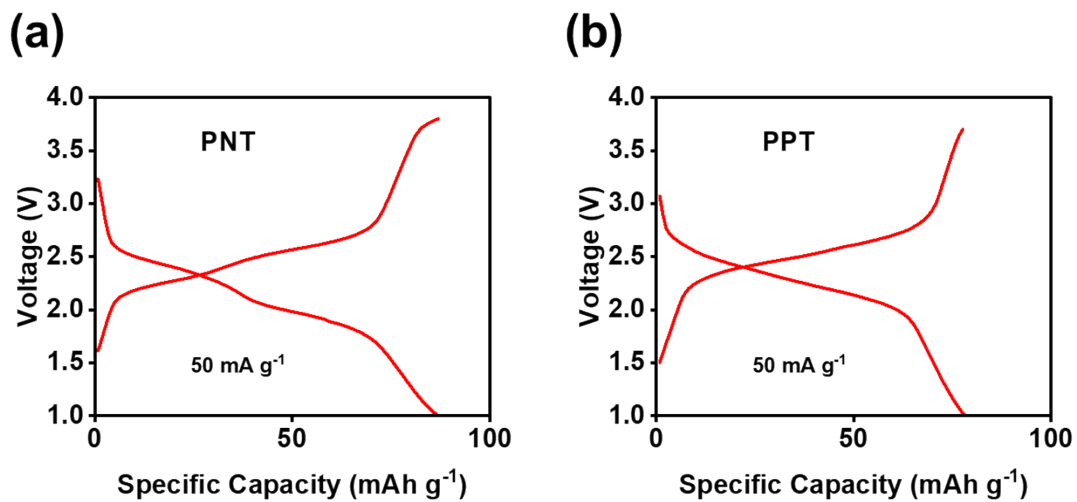


Fig. S13 Galvanostatic charge–discharge curves at the 150th cycle in KIBs: (a) PNT, (b) PPT.

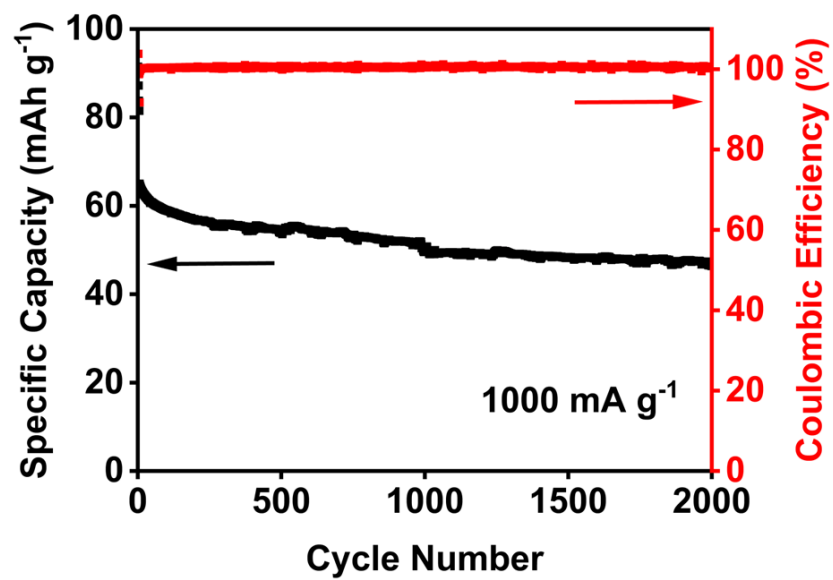


Fig. S14 De-potassiation capacity and Coulombic efficiency for PPT/single-layer graphene in KIBs.

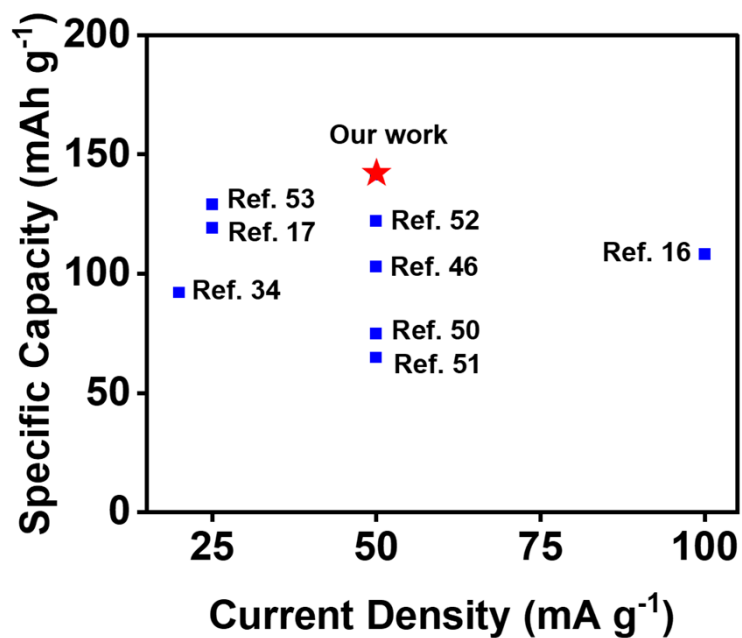


Fig. S15 Summary plot for the comparison of the specific capacity of our designed polymer with the previously reported organic compounds in alkali-ion batteries. Data from references 16, 17, 34, 46, 50, 51, 52, 53, and this work.

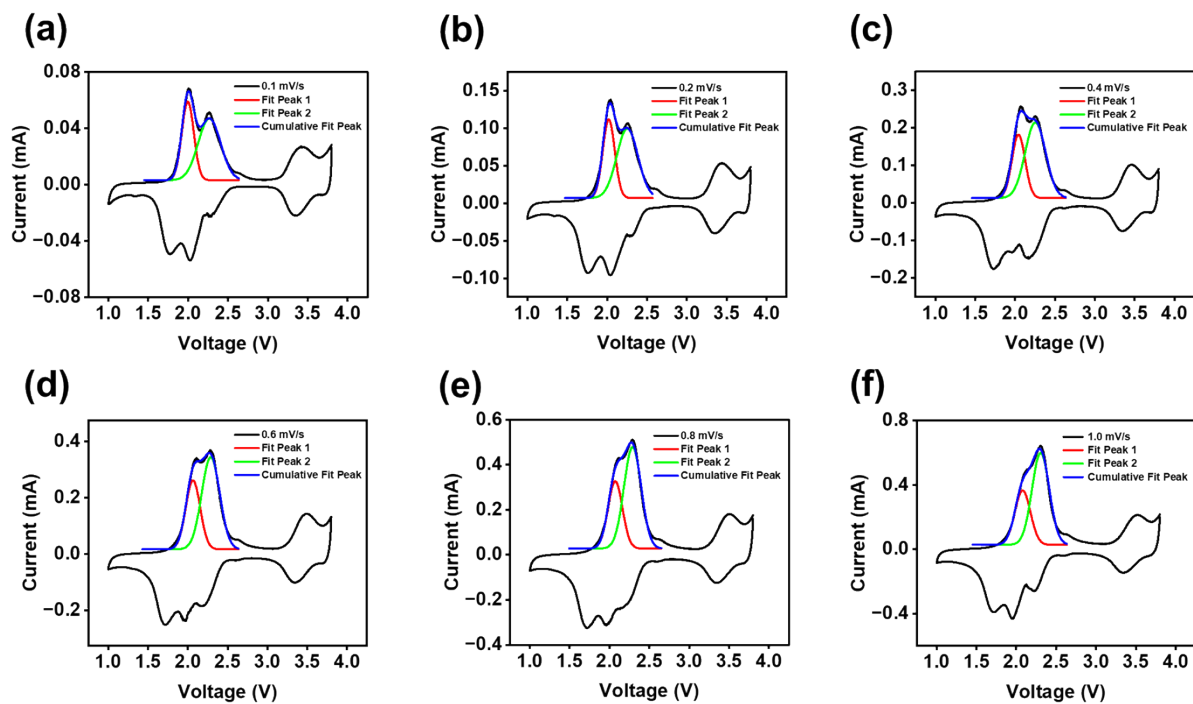


Fig. S16 Anodic peak deconvolution on cyclic voltammograms at different scan rates for PNT with single-layer graphene in NIBs.

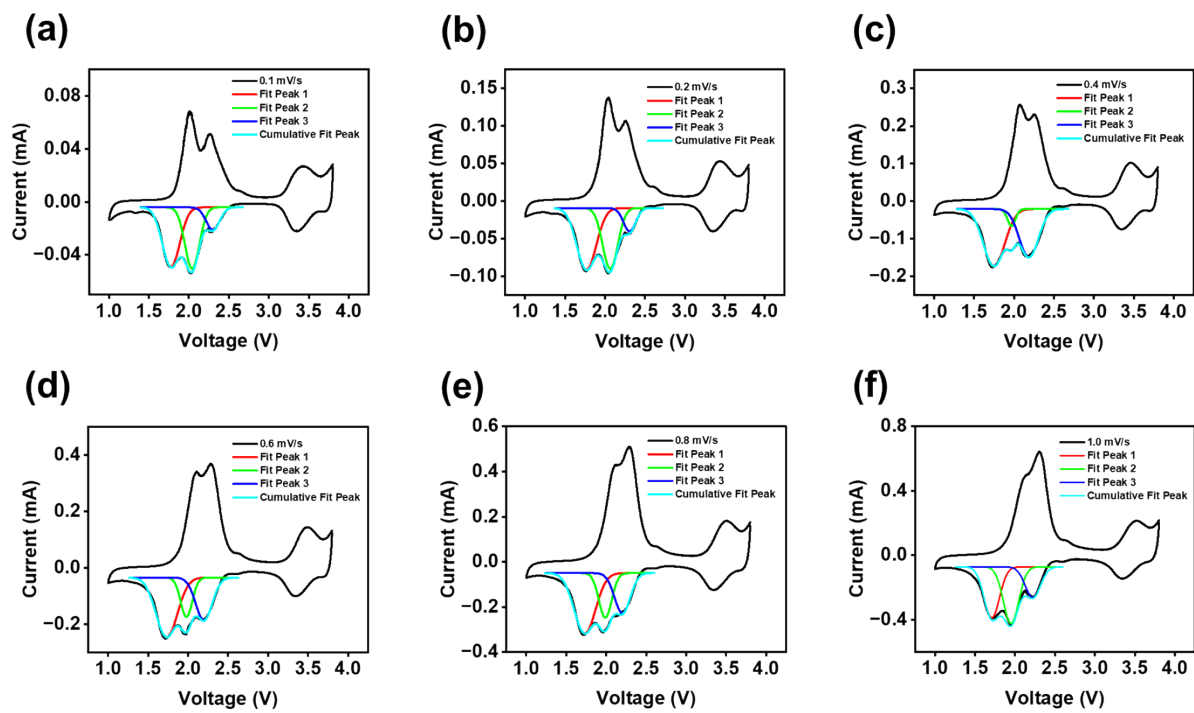


Fig. S17 Cathodic peak deconvolution on cyclic voltammograms at different scan rates for PNT with single-layer graphene in NIBs.

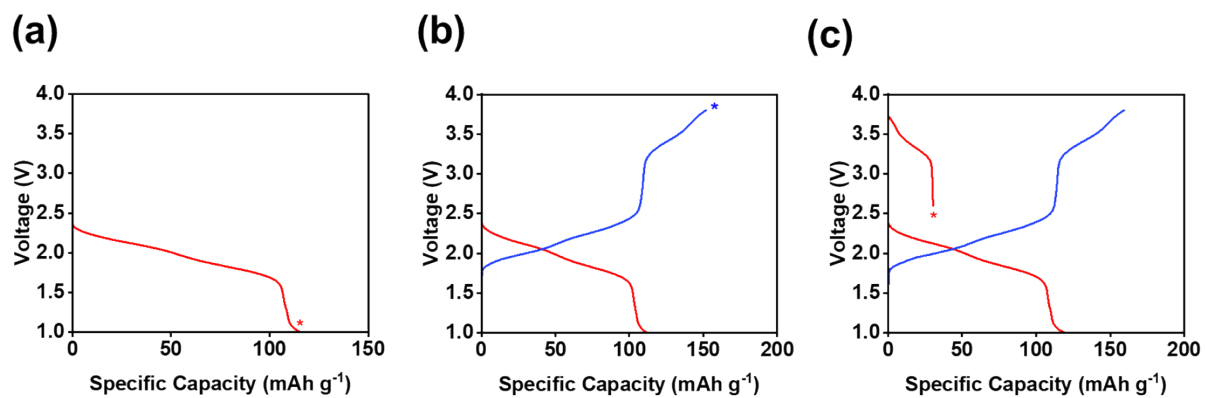


Fig. S18 Different stages of charge/discharge for the PNT electrode tested at the current density of 20 mA g⁻¹ for XPS analyses: (a) discharged to 1 V, (b) charged to 3.8 V, discharged to 2.6 V.

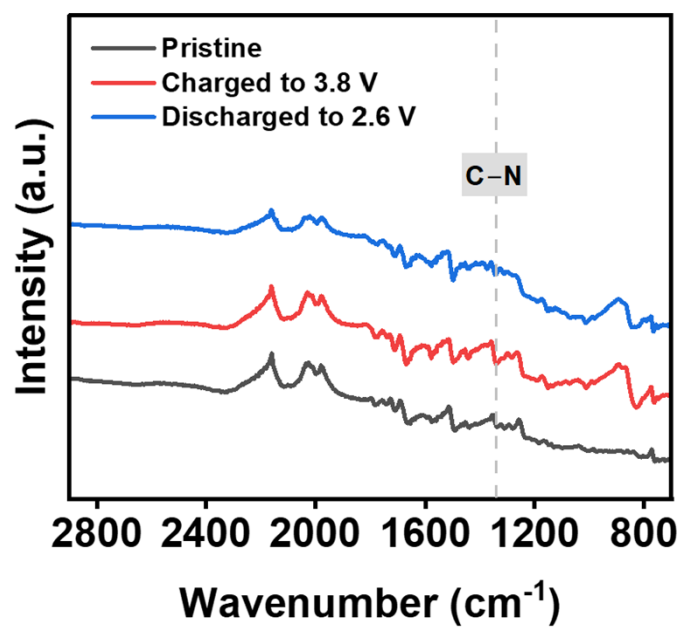


Fig. S19 FTIR spectra of the pristine and charged/discharged PNT electrodes.

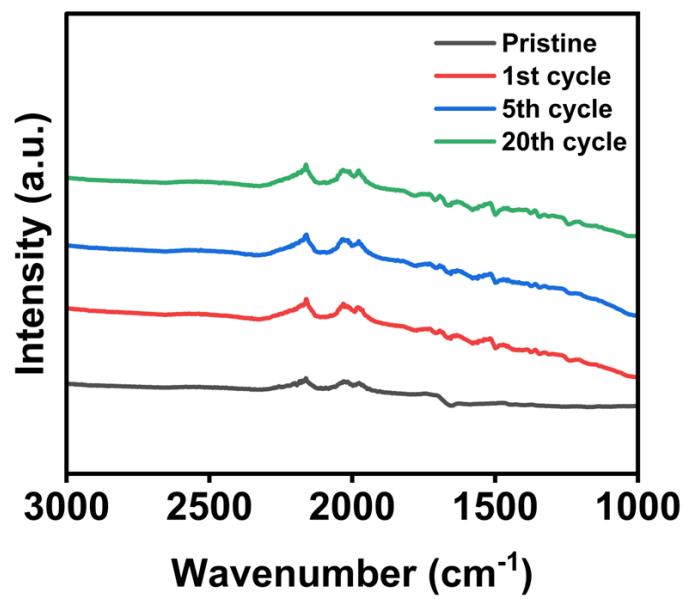


Fig. S20 FTIR spectra for PNT cathodes in NIBs after cycling.